Interaction of lysozyme with a tear film lipid layer model: a molecular dynamics simulation study

Alicja Wizert,[1] D. Robert Iskander,[1] and Lukasz Cwiklik[2,*]

[1]Department of Biomedical Engineering, Faculty of Fundamental Problems of Technology, Wroclaw University of Science and Technology, Wroclaw, Poland

[2]J. Heyrovský Institute of Physical Chemistry, Czech Academy of Sciences, v.v.i., Prague, Czech Republic

[*]*corresponding author: lukasz.cwiklik@jh-inst.cas.cz (L.C.)*

Abstract

Tear film is a thin multilayered structure covering the cornea. Its outermost layer is coated by a lipid film residing at the aqueous subphase. This tear film lipid layer (TFLL) is itself a complex structure, formed by both polar and nonpolar lipids. It was recently suggested that due to tear film dynamics, TFLL contains inhomogeneities in the form of polar lipid aggregates. The aqueous phase of tear film contains lachrymal-origin proteins, with lysozyme being one of the most abundant. These proteins were demonstrated to alter TFLL properties, mainly by reducing its surface tension. However, a detailed nature of protein-lipid interactions in tear film is not known. By employing coarse grain molecular dynamics simulations, we investigate in molecular details interactions of lysozyme with TFLL. We demonstrate that lysozyme, due to lateral restructuring of TFLL, is able to penetrate the tear lipid film embedded in inverse micellar aggregates.

Keywords:

Tear film; Tear film lipid layer; Lysozyme; Molecular dynamics

Introduction

Tear film is a thin layer of fluid that covers the eye. Tear film is important to the health and optics of the eye and it forms a barrier against the outside environment [1, 2]. The molecular composition of tear film is being better and better understood and provides knowledge about tear film dynamics [3], mechanisms of its instabilities [4], interactions of tear film with contact lens material [5, 6], and the etiology of the dry eye disease [7]. Human tear film is rich in proteins. In studies of Green-Church et al. [8] and Souza et al. [9], 97 and 491 unique proteins have been identified in the human tear film, respectively. That number has been recently increased to 1543 proteins [10]. From that large number, lipocalin, lysozyme and lactoferrin take up to about 80% of the total protein concentration. Lipocalin, previously known as prealbumin [11], is a major protein of the tear fluid that is also present in other body fluids and found in other species [12]. It comes from a family of lipid-binding proteins, appears to lower tear surface tension [13] and acts as a scavenger protecting epithelium [14]. Lysozyme constitutes approximately 20 to 40% of the total tear protein [15]. It is an antibacterial protein with a major role to equip the eye with resistance to infection [16]. A reduction of lysozyme in tear film has been associated with several eye diseases including dry eye [17], where a reduction of tear lipocalin is also observed [18], herpetic eye [19], and observed in patients prescribed with beta blockers [20]. Finally, a less populated lactoferrin plays an important role in the maintenance of ocular health, particularly in relation to immunological protection [21]. It has been suggested that quantification of each of those three major tear proteins could serve as a single supplemental biomarker for assessing ocular surface [18, 22].

In the classical three-layer model of tear film, tear proteins of lachrymal origin are present in the aqueous layer, which is covered by the outer lipid layer, so-called Tear Film

Lipid Layer (TFLL) [23, 24]. This lipid structure is fundamental for maintaining tear film stability. Its function is typically associated with ability to reduce surface tension of tear film [11]. Moreover, it is assumed that TFLL reduces friction during blinks, promotes tear film re-spreading, and reduces tears evaporation [25]. A typical model of tear film organization assumes that TFLL forms a relatively flat multilayered structure atop the aqueous subphase [23]. As demonstrated in our previous MD simulations [26, 27], such a lipid arrangement can be expected to exist under relaxed static conditions. However, lateral compression and decompression of the lipid layer resulting from eye blinks cause tear film to undergo a constant restructuring. This leads to formation of three-dimensional lipid structures [28-30], some of them in a form of polar lipid aggregates, both in the water subphase and in nonpolar layers of TFLL [26]. Those of the aggregates that reside in nonpolar layers typically resemble inverse micellar structures and may serve as polar lipid reservoirs during tear film restructuring.

Biological lipid layered structures are typically not of a purely-lipid type but contain numerous and often specific proteins. For instance, plasma membrane which structurally is made of a lipid bilayer as well as the pulmonary surfactant that is basically formed by a lipid monolayer are both rich in proteins [31]. Similarly, it was observed that lipid-protein interactions play a role in TFLL. In particular, experiments show that tear film proteins add to reducing surface tension by adsorbing to, or even penetrating the outer lipid layer [32, 33]. However, the mechanisms of such adsorption or penetration and, in general, the issues related to protein-lipid interaction in tear film, are presently not well understood.

The main protein known for altering TFLL properties is lysozyme [33]. One of the recommendations of the International Workshop on Meibomian Gland Dysfunction [7] is to focus future studies on finding interactions between the lysozyme and tear lipids and to ascertain whether structural changes in the lipid layer caused by lower lysozyme

3

concentration, could lead to increased rates of evaporation. Hence, the aim of this study is to evaluate the interactions between the lysozyme molecules and TFLL using the recently developed realistic model of tear film lipid layer [26] in the framework of coarse grain molecular dynamics (MD) simulations.

Methodology

The considered model of TFLL consisted of a mixture of polar and non-polar lipids simulated at the water-air interface. Polar lipids were chosen to mimic the experimentally obtained lipidome of the tear film [34]. These polar components included 1-palmitoyl-2-oleoyl-phosphatidylcholine (POPC), 1 palmitoyl-2-oleoyl-phosphatidylethanolamine (POPE), N-palmitoyl-D-erythro-sphingosine (Cer), and N-palmitoyl-D-erythro-sphingosyl-phosphorylcholine (SM). The non-polar lipids were modeled by a mixture of glycerine trioleate (TO) and cholesteryl oleate (CO) which are the two most abundant non-polar lipids as observed experimentally [23]. MD simulations were carried out employing the coarse grain MARTINI force field [35]. It enables simulation length- and timescales required for description of multicomponent lipid films under varying conditions while providing a near-atomistic description of considered molecular species. The MARTINI force field was previously successfully used for the description of lipid films [36-38], including TFLL models [26-28, 39, 40]. Lipid force field parameters were taken from the MARTINI library while the missing Cer parameterization was obtained by using SM residue with the headgroup beads exchanged to a single bead of P1 type [35]. The molecular structure of lysozyme from the Protein Data Bank (PDBID: 1HEL) was employed [41], and the MARTINI coarse grain representation of the protein (both structure and topology) was created using martnize.py tool . The elastic network approach was employed with the elastic

bond force constant set to 500 kJ·mol^{-1}·nm^{-2} and lower and upper elastic bond cut-off to 0.5 and 0.9 nm, respectively. Finally, the protein structure was minimized, solvated, and simulated for 100 ns for equilibration purposes, with root mean square displacements used to control the equilibration. The ability of the elastic network constraints to maintain the structure of protein during its interaction with lipid film was confirmed (see Fig. S1 in SI).

Simulations of the TFLL model were performed in the periodic box containing a slab of water placed in the middle of the box. The box was elongated in one direction hence forming two independent air-water interfaces. Two lipid films of the same composition were placed at both interfaces. The presence of two interfaces allows for obtaining better statistics as two system replicas are simulated during a single simulation run. Such a simulation box setup is standardly used in lipid film studies. Two systems with different sizes were considered in simulations, with either about 87,000 or about 630,000 water beads in the slab. Note that each water bead in the MARTINI model represents four actual water molecules. The large simulation box contained in total (at two interfaces) 25,600 lipid molecules (5,824 polar and 19,776 nonpolar). The composition of the polar subphase (in mol percent: POPC – 68%, POPE – 22%, SM – 5%, Cer – 5%) was chosen to approximately correspond to the experimental lipidome [34]. The number of nonpolar lipids was chosen as to be able to form a relatively thick multilayer at the interface. The nonpolar subphase had roughly equimolar ratio of TO and CO. In the small variant of the simulation box, the number of lipids was scaled down to 6,400 lipid molecules. We employed area per polar lipid (APPL, defined as the number of polar lipids at the interface divided by the interface area) to characterize lateral packing of lipids. The sizes of the boxes were 47·47·104 nm^3 and 22·22·104 nm^3. These values corresponded to APPL=0.67 nm^2; in some of simulations the boxes were further laterally compressed to reduce APPL, maximally down to APPL=0.45 nm^2. The above-described system setup regarding the lipid film corresponds to the setup that was employed in

our previous study [26] but here larger lateral box sizes are considered because of the presence of the protein.

Molecules of lysozyme were introduced in the water phase, approximately in the middle of the slab in order to avoid initial protein-TFLL interactions. Either a single or up to 33 proteins were considered. Chloride counterions (eight per each lysozyme molecule) were introduced to neutralize the protein charge. As we verified, the ions during simulations were not in direct permanent contact with the protein. The systems were shortly equilibrated (tens of nanoseconds) upon introduction of the protein; note that this equilibration timescale is much shorter than the timescale of protein diffusion toward the interface.

MD simulations were performed employing the GROMACS 4.6.5 software suit [42] using a standard protocol advised for MARTINI simulations with this version of GROMACS [43]. Namely, 1.1 nm cut-off was employed for non-bonded interactions using the potential-shift-Verlet method implemented in GROMACS. The reaction-field algorithm was used to account for long-range electrostatics with the relative electrostatic screening parameter equal to 15. Equations of motions were integrated with 10 fs time step. The temperature of 310 K was controlled using the velocity rescale algorithm with 1.0 ps coupling parameter. Simulations with the fixed APPL were performed within the canonical ensemble with the size of the box kept constant. Trajectories of 500 ns were calculated with first 150 ns of each simulation treated as equilibration. Different variants of non-equilibrium simulations of lateral squeezing of the interfacial film were also performed, with lateral compression realized by employing semi-isotropic barostat algorithms (either Berendsen or Parrinello-Rahman) with the pressure between 1 to 3 bars [44, 45]. The simulation time in this case varied between 140 and 900 ns. Free-energy profiles of protein penetration into the lipid film were calculated from potential of mean force obtained employing the umbrella sampling MD simulations [46]. The distance

between the protein center of mass and the water slab mid-plane was used as a reaction coordinate. Initial windows configurations with the spacing of 0.1 nm were generated by the pulling algorithm employing the force constant of 3,000 kJ·mol^{-1}·nm^{-2} and the pull rate of 0.008 nm·ps^{-1}. Each window was then simulated for 50 ns with the reaction coordinate restrained using harmonic force with 3,000 kJ·mol^{-1}·nm^{-2} force constant. Initial 25 ns were treated as equilibration, therefore, not used in further analysis. Weighted Histogram Analysis Method was then used to extract potential of mean force [47]. Standard GROMACS tools were used for trajectory analysis while visualization was performed using VMD software [48].

Results and discussion

Lysozyme adsorption to the TFLL

Interactions of lysozyme with the TFLL model were first studied in the presence of the laterally relaxed TFLL. To this end, the film with APPL=0.67 nm^2 was employed and either one or several lysozyme molecules were initially placed in the water sub-phase. In the course of these simulations, each few hundreds of ns-long, proteins were predominantly occupying the water phase. Nevertheless, several events of transient contact of the protein with TFLL lipids were observed. These contacts were occurring at the water-lipid interface without penetration of the protein in-between lipids. A typical snapshot from a simulation capturing the lysozyme-lipids contact is shown in Fig. 1. To estimate free energy of lysozyme adsorption at the water-lipid interface as well as its penetration into the TFLL, additional MD simulations were performed employing the umbrella sampling method. The snapshots corresponding to this pulling simulation are presented in Fig. 2. In Fig. 3a, a free energy profile corresponding to lysozyme transfer between the water phase and TFLL is presented.

The free energy curve demonstrates that there is a shallow (about 4 kJ/mol) free energy minimum corresponding to lysozyme adsorption at phospholipid headgroups. Hence, it indicates that there is a weak preference for lysozyme adsorption at the water-lipid interface. This is in accord with the experimental study where weak adsorption of lysozyme at lipid headgroups in monolayer systems was observed [33]. In that study, adsorption was dependent on the chemical identity of lipid headgroups with zwitterionic ones interacting with the protein somewhat less than the charged ones. In our model, only neutral headgroups are present hence the observed weak adsorption is in accord with the previous experimental work. Further penetration of lysozyme into TFLL leads to reduction of contacts with polar lipids and increase of contact with their nonpolar counterparts, as seen in Fig. 3b. Such a penetration is strongly prohibited as demonstrated by the steep increase of the free energy in this region. This can be rationalized by the tendency of the relatively hydrophilic lysozyme to avoid nonpolar environments.

An analysis of contacts between the adsorbed lysozyme and lipids is presented in Fig. 4. In the case of laterally-relaxed interface (Fig. 4a), most of contacts are formed between the protein and both PC and PE headgroups as these lipids are the most abundant. Still, there are a significant number of protein-ceramide contacts while contacts with SM and CO are very minor. When different sizes of lipid populations at the interface are accounted for (by means of normalization to the number of polar lipids of a given type, see Fig. S2 in SI), it is clear that lysozyme-lipid binding propensity follows the trend Cer>PE>PC>>SM~CO. The significant binding to Cer is somewhat surprising as other headgroups, in particular those of SM, are relatively well exposed at the lipid-water interface in comparison with the small Cer headgroups that are typically buried between other lipid molecules [27]. Note that in the experimental study [33] neither SM nor Cer were

investigated. Number of contacts formed with the lipids by individual lysozyme residues is quantified in Fig. 5. Residues 46-50 and 61-75 preferentially interact with both PC and PE headgroups while Cer is interacting mainly with residues 65-74. All these residues are well exposed to water and are predominantly of hydrophilic character. Note that in lysozyme, almost all residues are well hydrated (see Fig. 5, bottom panel), this is because of the hydrophilic nature of the protein. The transient adsorption to the lipid film does not significantly reduce hydration of the lipid-bound residues. In the previous coarse grain MD work on lysozyme adsorption at variously decorated surfaces [49], lysozyme was adsorbed specifically at a hydrophilic interface built of 1-nonadecanol chains attached to a solid sub-surface with specific contact involving mostly residues: LYS1, ARG5, ARG114, LYS116, ARG125, ARG128. The difference between those results and our data can be rationalized by a complex and dynamic nature of the lipid mixture used here as a TFLL model where the interface is formed by several headgroup types of varying chemical character.

An analysis of lysozyme interactions with the laterally compressed undulated TFLL films in MD simulations is difficult because of limited sampling of various surface topological details. Number of protein-lipid contacts calculated in such a system is presented in Fig. 4b (the data taking into account different lipid population sizes are shown in Fig. S2 in SI). In this 2.4 μs-long simulation at APPL=0.45 nm^2, lysozyme was located in the vicinity of variously curved water-lipid interfaces. As evident, numbers of protein-lipid contacts resemble those under laterally relaxed conditions (Fig. 4a) with the main difference being more abundant protein-SM contacts. Note that we have previously shown that lateral squeezing of TFLL does not lead to increased presence of the SM headgroup at the water-lipid interface [27] hence this is a specific effect related to protein-SM interactions. Contacts of individual lysozyme residues with lipids and water are presented in Fig. S3 in SI. Increased polar lipid binding by residues located close to both terminals is visible. The

residues between 46 and 74, bonded under laterally relaxed conditions (see Fig. 5) are not of key importance here. Note, however, that due to limited sampling of various protein-lipid configurations in the curved system this binding preferences should be treated cautiously.

Lysozyme encapsulation in the laterally squeezed TFLL

In our previous in silico study of TFLL, we observed formation of various lipid structures upon lateral compression of TFLL [26]. In particular, micelles of polar lipids detached from the interface and occupying the water phase were observed. Such a process resembles a typical scenario where a polar lipids monolayer collapses [37]. Moreover, we observed formation of inverse micellar structures consisting of polar lipids and encapsulated water, a process that does not occur in the monolayer case. These inverse micelles either remained adsorbed at the polar-nonpolar interface or were transferred into the nonpolar lipid phase. Here, we evaluated behavior of lysozyme during the process of the water-lipid interface restructuring. To this end, we performed several (thirty-two) non-equilibrium MD simulations of TFLL lateral compression with lysozyme present in the vicinity of the TFLL. Among these simulations, in more than half cases (nineteen) we observed that the protein that was initially adsorbed at the water-lipid interface underwent (to a various extent) incorporation into the restructured polar lipid layer. Representative snapshots of such incorporation are shown in Fig. 6. Moreover, in three of these trajectories we observed full encapsulation of the protein in an inverse micelle; one such a case is depicted in Fig. 7.

To gain a more quantitative insight into the encapsulation process, we analyzed the protein-lipid neighbors. In Figs. 8a and 8b, lipids located at distances 0.8 and 2.5 nm from encapsulated lysozyme are depicted. It is evident that the nearest-distance criterion used for typical contact analysis (0.8 nm) does not capture the inverse micelle lipids. In Fig. 7c, radial

distribution functions calculated between the protein, polar lipids, nonpolar lipids, and water obtained upon lysozyme encapsulation are depicted; for comparison, the same data for protein adsorbed at the interface at APPL=0.67 nm^2 where no encapsulation was observed are shown in Fig. 8d. Upon encapsulation, the closest neighbors of the protein (<0.8 nm that approximately corresponds to the position of the first minimum in the radial distribution function) are water and polar lipids. This can be rationalized by the fact that the lysozyme enclosed in the inverse micelle is still hydrated but some of atoms of polar lipids forming the micelle replace water in the first solvating shell of the protein. Note that in the non-encapsulated case, there is more hydrating water but still lipids are on average present close to the lysozyme; the latter occurring because the protein is adsorbed at the water-TFLL interface. After encapsulation, nonpolar lipids reside at relatively large distance from the protein; cholesteryl ester at >1.2 nm and triglyceride at >1.5 nm. These distances correspond to the separation between the protein and nonpolar lipids by the polar lipid capsule. The somewhat closer distance to CE than that to TG is in accord with the results obtained in our previous studies [26, 27] where partial penetration of CE to the polar lipids monolayer was observed. Similar arrangement of nonpolar lipids is visible in the non-encapsulated case, but the distances from protein are significantly larger, in particular that of TG. It is because CE penetrates easier between polar lipids than TG.

In order to further quantify the protein encapsulation process in the inverse micelles, we analyzed the number of contacts between the protein and individual classes of polar lipids. In Fig. 9, the contacts between lysozyme and lipid atoms as well as with water are presented within the distance of 2.5 nm from protein corresponding to inverse micelle-forming lipids. The data obtained in three non-equilibrium MD trajectories with different rate of lysozyme incorporation are presented. The curves are normalized to take into account different populations of lipid types (for not normalized data see Fig. S4 in SI). In the slowest

case (Fig. 9a), up to about 120 ns, there is approximately constant (in time) number of contacts between the protein and polar lipids as well as between the protein and water. At about 120 ns, contacts with polar lipids become more abundant. This corresponds to entrapment of the protein in the fold of polar lipids that starts to form at the water-TFLL interface. This trend continues till about 300 ns. At the same time, the number of protein-water contacts decreases; corresponding to partial dehydration of the protein during incorporation in the polar lipids bulge. At >300 ns, the number of protein-polar lipids contacts is diminished while protein hydration increases. This corresponds to formation of a "mature" inverse micelle enclosing the protein along with some of protein-hydrating water. The snapshots depicting the discussed states observed along the trajectory are depicted in Fig. 7.

Note, that the number of protein-water contacts is similar to that before encapsulation while the number of polar lipids in the vicinity of the protein is significantly increased. Even more importantly, there is some specificity between protein-lipid contacts during the encapsulation process. Namely, the prevailing are the lysozyme-sphingomyelin contacts and, to a lesser extent, lysozyme-phosphatidylcholine ones. Note that the data are normalized to the numbers of individual lipid types present at the interface. Hence, the differences between the curves represent different preferences in protein-lipid contacts. In Figs. 9b and 9c, the contacts data obtained during two MD trajectories with a faster encapsulation process are shown. Qualitatively, these plots show the same features as in the slow encapsulation case, with transient protein dehydration accompanied by a steep increase of protein-lipid contacts, followed by reduction of some of them with protein re-hydration occurring. Notably, protein-sphingomyelin contacts prevail in all cases during the encapsulation process. We also analyzed the protein-lipid contacts at the distances up to 0.8 nm (Fig. S5 in SI) that correspond to the nearest neighbors of the protein. Similar to the longer-distance data (Fig.

9), the rise of protein-sphingomyelin contacts is dominant. Even though there is transient increase of protein-ceramide contact number in one of the trajectories (Fig. S5a), protein-sphingomyelin ones dominate in later phases of encapsulation.

The analysis of contacts between individual amino acids and lipids does show a crowding effect (see Fig. 6 in SI). Namely, there is overall more protein-lipid contact in the case of the encapsulated lysozyme (compare Figs. 4a and 4b with Fig. S6a). Interestingly, there are numerous contacts of lysozyme with both SM and Cer, similar to the case of undulated TFLL without encapsulation (Fig .4b). It suggests that this is the curvature of the lipid film that enhances contacts of these lipids with the protein. We observed no specific preferences of lipid binding by individual lysozyme residues. The latter is similar to the case of the non-encapsulated protein adsorbed at the flat water-lipid interface.

Conclusions

Tear film lipid layer is typically associated with its role for maintaining tear film mechanical stability by decreasing surface tension. It resides at the aqueous phase that is rich in water soluble proteins, in particular, the most abundant lysozyme that plays a key role in antimicrobial defense of the eye. In earlier experimental studies, lysozyme was shown to alter TFLL properties. Previous MD simulations suggest that TFLL, apart from being a multilayered structure of polar and nonpolar lipids, contains lipid aggregates in inverse micellar form.

Here, by employing coarse grain MD simulations of TFLL model with lysozyme present in the water subphase, we demonstrate that the hydrophilic protein that typically resides in the aqueous tear film sub-phase can undergo embedding into micelle-like lipid structures in TFLL. Such a process occurs as a consequence of the lateral restructuring of the

film and requires that a protein molecule is initially present in the vicinity of TFLL. As we show, the latter condition is fulfilled for lysozyme. It can be envisaged, that this mechanism is not restricted to lysozyme but should be operative for any hydrophilic molecule. Hence, TFLL may effectively act as a solvent and reservoir of hydrophilic species.

Note that encapsulation requires the protein to be present in the vicinity of the invagination formed during polar lipid layer restructuring. This condition is not fulfilled for all proteins adsorbed at the interface, as demonstrated by the fact that not all MD trajectories calculated with adsorbed lysozyme led to its encapsulation. Nevertheless, in the actual tear film, where the number of lysozymes in the vicinity of the water-lipid boundary is high and TFLL restructuring occurs persistently due to eye blinks, we predict that the lysozyme encapsulation process is likely to be frequent.

Encapsulation of a molecule by inverse micelles in TFLL is, in principle, a reversible process. Once concentration of such micelles is high, lateral restructuring of TFLL, in particular, film decompression, may lead to break up of inverse micelles and subsequent transfer of hydrophilic molecules to the aqueous sub-phase. Note that some of the inverse micelles with embedded protein should be able to detach from the polar lipids layer and diffuse into the nonpolar lipids region. Such a process was demonstrated to occur for inverse micelles without the protein in our previous study. This phenomenon would lead to enrichment of TFLL in hydrophilic lysozyme and this may potentially boost tears antimicrobial activity already in the outermost nonpolar, layer of the tear film.

In simulations, sphingomyelin plays an assisting role during protein encapsulation. Namely, the contacts between lysozyme and SM are particularly frequent during initial formation of the lipid bulge and its subsequent 'maturing' toward inverse micelles. Such a behavior of sphingomyelin during lysozyme incorporation is in accord with significant presentation of SM headgroups at the water-TFLL interface demonstrated in the recent study

[27]. It would be particularly interesting to address the role of SM experimentally employing a model system with a well-controlled lipid film composition.

The predicted ability of nonpolar TFLL to incorporate hydrophilic molecules has several consequences. First, if the encapsulated molecule is a protein, its function may occur already in the TFLL. In the case of lysozyme, this would lead to modulation of innate immunological response of the tear film. Second, the presence of encapsulated polar species would alter biophysical properties of TFLL, such as its mechanical stability and water permeability. Third, encapsulation of water-soluble species in TFLL seems important from drug delivery point of view. For instance, retention time of a drug in the tear film can be enhanced because of its entrapment in TFLL, or inverse micellar form can be used for accumulation and subsequent delivery of a molecule via TFLL to the aqueous subphase.

Supporting Information

Supplementary figures with analysis of MD trajectories.

Acknowledgements

Competing Interests: The authors have declared that no competing interests exist.

References

1.   Sweeney DF, Millar TJ, Raju SR. Tear film stability: a review. Exp Eye Res. 2013;117:28-38.

2.   Montés-Micó R. Role of the tear film in the optical quality of the human eye. Journal of Cataract & Refractive Surgery. 2007;33(9):1631-5.

3.   Khanal S, Millar TJ. Nanoscale phase dynamics of the normal tear film. Nanomedicine-Nanotechnology Biology and Medicine. 2010;6(6):707-13.

4.   Lam SM, Tong L, Reux B, Duan X, Petznick A, Yong SS, et al. Lipidomic analysis of human tear fluid reveals structure-specific lipid alterations in dry eye syndrome. J Lipid Res. 2014;55(2):299-306.

5.   Craig JP, Willcox MD, Argüeso P, Maissa C, Stahl U, Tomlinson A, et al. The TFOS International Workshop on Contact Lens Discomfort: Report of the Contact Lens Interactions With the Tear Film SubcommitteeReport on Interactions With Tear Film. Investigative ophthalmology & visual science. 2013;54(11):TFOS123-TFOS56.

6.   Masoudi S, Stapleton FJ, Willcox MDP. Contact lens-induced discomfort and protein changes in tears. Optometry & Vision Science. 2016;93(8):955-62.

7.   Green-Church KB, Butovich I, Willcox M, Borchman D, Paulsen F, Barabino S, et al. The international workshop on meibomian gland dysfunction: report of the subcommittee on tear film lipids and lipid-protein interactions in health and disease. Invest Ophthalmol Vis Sci. 2011;52(4):1979-93.

8.   Green-Church KB, Nichols KK, Kleinholz NM, Zhang L, Nichols JJ. Investigation of the human tear film proteome using multiple proteomic approaches. 2008.

9.   de Souza GA, de Godoy LM, Mann M. Identification of 491 proteins in the tear fluid proteome reveals a large number of proteases and protease inhibitors. Genome biology. 2006;7(8):R72.

10.   Zhou L, Zhao SZ, Koh SK, Chen L, Vaz C, Tanavde V, et al. In-depth analysis of the human tear proteome. Journal of proteomics. 2012;75(13):3877-85.

11.   Bron AJ, Tiffany JM, Gouveia SM, Yokoi N, Voon LW. Functional aspects of the tear film lipid layer. Experimental Eye Research. 2004;78(3):347-60.

12.   Redl B. Human tear lipocalin. Biochimica et Biophysica Acta (BBA)-Protein Structure and Molecular Enzymology. 2000;1482(1):241-8.

13.   Nagyova B, Tiffany JM. Components responsible for the surface tension of human tears. Current eye research. 1999;19(1):4-11.

14.   Glasgow BJ, Marshall G, Gasymov OK, Abduragimov AR, Yusifov TN, Knobler CM. Tear lipocalins: Potential lipid scavengers for the corneal surface. Investigative Ophthalmology & Visual Science. 1999;40(13):3100-7.

15.   Shamsi FA, Chen Z, Liang J, Li K, Al-Rajhi AA, Chaudhry IA, et al. Analysis and comparison of proteomic profiles of tear fluid from human, cow, sheep, and camel eyes. Investigative ophthalmology & visual science. 2011;52(12):9156-65.

16.   Grabner G, Formanek I, Dorda W, Luger T. Human tear lysozyme. Graefe's Archive for Clinical and Experimental Ophthalmology. 1982;218(5):265-70.

17.   Versura P, Nanni P, Bavelloni A, Blalock W, Piazzi M, Roda A, et al. Tear proteomics in evaporative dry eye disease. Eye. 2010;24(8):1396-402.

18.   Caffery B, Joyce E, Boone A, Slomovic A, Simpson T, Jones L, et al. Tear lipocalin and lysozyme in Sjögren and non-Sjogren dry eye. Optometry & Vision Science. 2008;85(8):661-7.

19.   Eylan E, Ronen D, Romano A, Smetana O. Lysozyme tear level in patients with herpes simplex virus eye infection. Investigative ophthalmology & visual science. 1977;16(9):850-3.

20.   Mackie I, Seal D, Pescod J. Beta-adrenergic receptor blocking drugs: tear lysozyme and immunological screening for adverse reaction. British Journal of Ophthalmology. 1977;61(5):354-9.

21.   Flanagan J, Willcox M. Role of lactoferrin in the tear film. Biochimie. 2009;91(1):35-43.

22.   Zhou L, Beuerman RW, Chan CM, Zhao SZ, Li XR, Yang H, et al. Identification of tear fluid biomarkers in dry eye syndrome using iTRAQ quantitative proteomics. Journal of proteome research. 2009;8(11):4889-905.

23.   Butovich IA. The Meibomian Puzzle: Combining pieces together. Prog Retin Eye Res. 2009;28(6):483-98.

24.   Cwiklik L. Tear film lipid layer: A molecular level view. Biochimica et Biophysica Acta (BBA)-Biomembranes. 2016;(10):2421-30.

25.   Yokoi N, Yamada H, Mizukusa Y, Bron AJ, Tiffany JM, Kato T, et al. Rheology of tear film lipid layer spread in normal and aqueous tear–deficient dry eyes. Investigative ophthalmology & visual science. 2008;49(12):5319-24.

26.   Wizert A, Iskander DR, Cwiklik L. Organization of Lipids in the Tear Film: A Molecular-Level View. Plos One. 2014;9(3).

27.   Olżyńska A, Cwiklik L. Behavior of sphingomyelin and ceramide in a tear film lipid layer model. Annals of Anatomy-Anatomischer Anzeiger. 2017;210:128-34.

28.   Kulovesi P, Telenius J, Koivuniemi A, Brezesinski G, Vattulainen I, Holopainen JM. The impact of lipid composition on the stability of the tear fluid lipid layer. Soft Matter. 2012;8(21):5826-34.

29.   Dwivedi M, Brinkkötter M, Harishchandra RK, Galla H-J. Biophysical investigations of the structure and function of the tear fluid lipid layers and the effect of ectoine. Part B: artificial lipid films. Biochimica et Biophysica Acta (BBA)-Biomembranes. 2014;1838(10):2716-27.

30.   Patterson M, Vogel HJ, Prenner EJ. The effect of repeated lateral compression and expansions mimicking blinking on selected tear film polar lipid monofilms. Biochimica et Biophysica Acta (BBA)-Biomembranes. 2017;1859(3):319-30.

31.   Edidin M. Lipids on the frontier: a century of cell-membrane bilayers. Nature Reviews Molecular Cell Biology. 2003;4(5):414-8.

32.   Saaren-Seppälä H, Jauhiainen M, Tervo TM, Redl B, Kinnunen PK, Holopainen JM. Interaction of purified tear lipocalin with lipid membranes. Investigative ophthalmology & visual science. 2005;46(10):3649-56.

33.   Mudgil P, Torres M, Millar TJ. Adsorption of lysozyme to phospholipid and meibomian lipid monolayer films. Colloids Surf B Biointerfaces. 2006;48(2):128-37.

34.   Rantamaki AH, Seppanen-Laakso T, Oresic M, Jauhiainen M, Holopainen JM. Human tear fluid lipidome: from composition to function. PLoS One. 2011;6(5):e19553.

35.   Marrink SJ, Risselada HJ, Yefimov S, Tieleman DP, de Vries AH. The MARTINI force field: coarse grained model for biomolecular simulations. The journal of physical chemistry B. 2007;111(27):7812-24.

36.   Baoukina S, Monticelli L, Amrein M, Tieleman DP. The molecular mechanism of monolayer-bilayer transformations of lung surfactant from molecular dynamics simulations. Biophys J. 2007;93(11):3775-82.

37.   Baoukina S, Monticelli L, Risselada HJ, Marrink SJ, Tieleman DP. The molecular mechanism of lipid monolayer collapse. Proc Natl Acad Sci U S A. 2008;105:10803-8.

38.   Marrink SJ, Tieleman DP. Perspective on the Martini model. Chemical Society reviews. 2013;42(16):6801-22.

39.   Telenius J, Koivuniemi A, Kulovesi P, Holopainen JM, Vattulainen I. Role of Neutral Lipids in Tear Fluid Lipid Layer: Coarse-Grained Simulation Study. Langmuir. 2012;28(49):17092-100.

40.   Kulovesi P, Telenius J, Koivuniemi A, Brezesinski G, Rantamaki A, Viitala T, et al. Molecular organization of the tear fluid lipid layer. Biophys J. 2010;99(8):2559-67.

41.   Wilson KP, Malcolm B, Matthews B. Structural and thermodynamic analysis of compensating mutations within the core of chicken egg white lysozyme. J Biol Chem. 1992;267(15):10842-9.

42.   Hess B, Kutzner C, van der Spoel D, Lindahl E. GROMACS 4: Algorithms for Highly Efficient, Load-Balanced, and Scalable Molecular Simulation. J Chem Theory Comput. 2008;4(3):435-47.

43.   De Jong DH, Baoukina S, Ingólfsson HI, Marrink SJ. Martini straight: Boosting performance using a shorter cutoff and GPUs. Computer Physics Communications. 2016;199:1-7.

44.   Berendsen HJC, Postma JPM, van Gunsteren WF, DiNola A, Haak JR. Molecular dynamics with coupling to an external bath. J Chem Phys. 1984;81(8):3684-90.

45.   Parrinello M, Rahman A. Polymorphic transitions in single crystals: A new molecular dynamics method. Journal of Applied Physics. 1981;52(12):7182-90.

46.   Kästner J. Umbrella sampling. Wiley Interdisciplinary Reviews: Computational Molecular Science. 2011;1(6):932-42.

47.   Kumar S, Rosenberg JM, Bouzida D, Swendsen RH, Kollman PA. The weighted histogram analysis method for free-energy calculations on biomolecules. I. The method. J Comput Chem. 1992;13(8):1011-21.

48.   Humphrey W, Dalke A, Schulten K. VMD: Visual molecular dynamics. Journal of Molecular Graphics. 1996;14(1):33-8.

49.   Yu G, Liu J, Zhou J. Mesoscopic Coarse-Grained Simulations of Lysozyme Adsorption. The Journal of Physical Chemistry B. 2014.

Figures
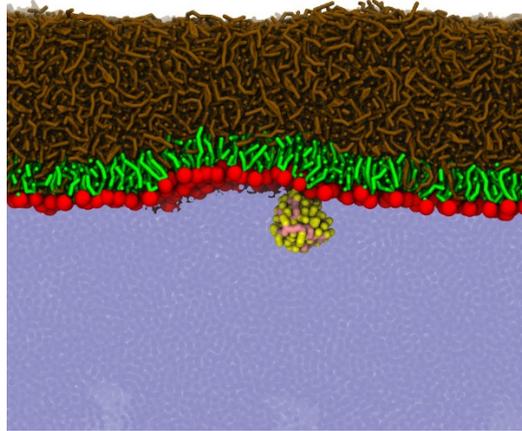
Fig. 1.Lisozyme adsorbed at the water-TFLL interface. A representative snapshot from equilibrium MD simulation is presented. Lysozyme is shown in yellow and pink, headgroups of polar lipids in red, tails of polar lipids in green, nonpolar lipids in brown, and water in blue.
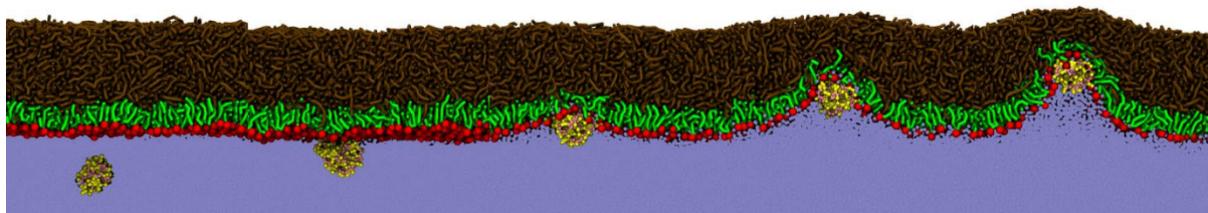
Fig. 2. Simulation snapshots taken along umbrella sampling simulations (time progresses from left to right) depicting the pulling of lysozyme molecule from water phase into TFLL. The figure combines initial snapshots from five selected representative umbrella sampling windows. For color coding see Fig. 1.
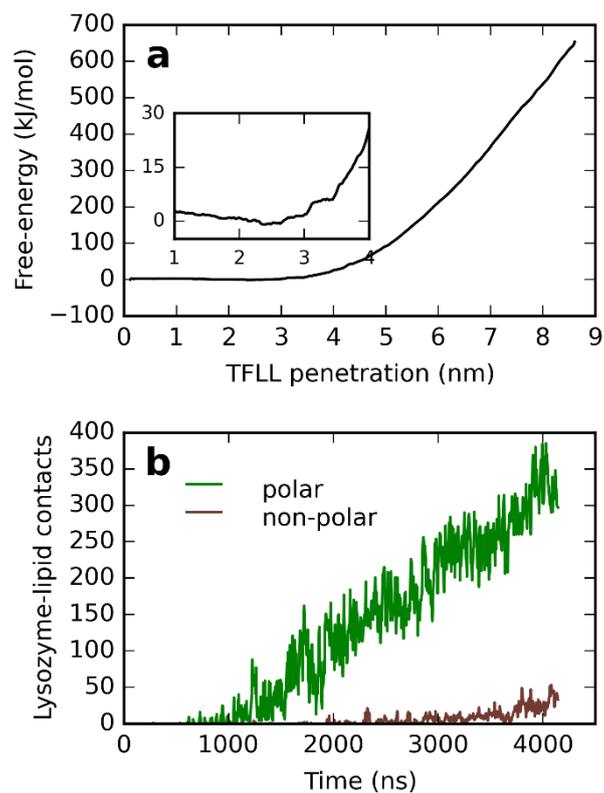
Fig. 3. Free-energy profile related to the lysozyme penetration into TFLL (a) and the number of lysozyme-lipid contacts (b) calculated using umbrella sampling MD simulations. The cumulative time from concurrent pulling widows as the protein progresses into the TFLL is shown in time axis. A magnification of the free energy curve is shown in the inset.
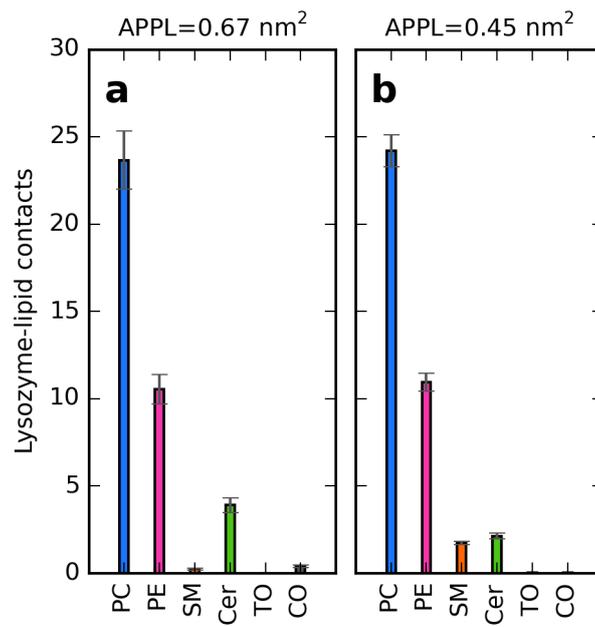
Fig. 4. Lysozyme-lipid contacts under equilibrium in laterally (a) relaxed and (b) compressed TFLL calculated employing 0.8 nm cutoff. Error bars represent standard error of the data. For the data normalized per number of individual polar lipid types, see Fig. S2 in SI.
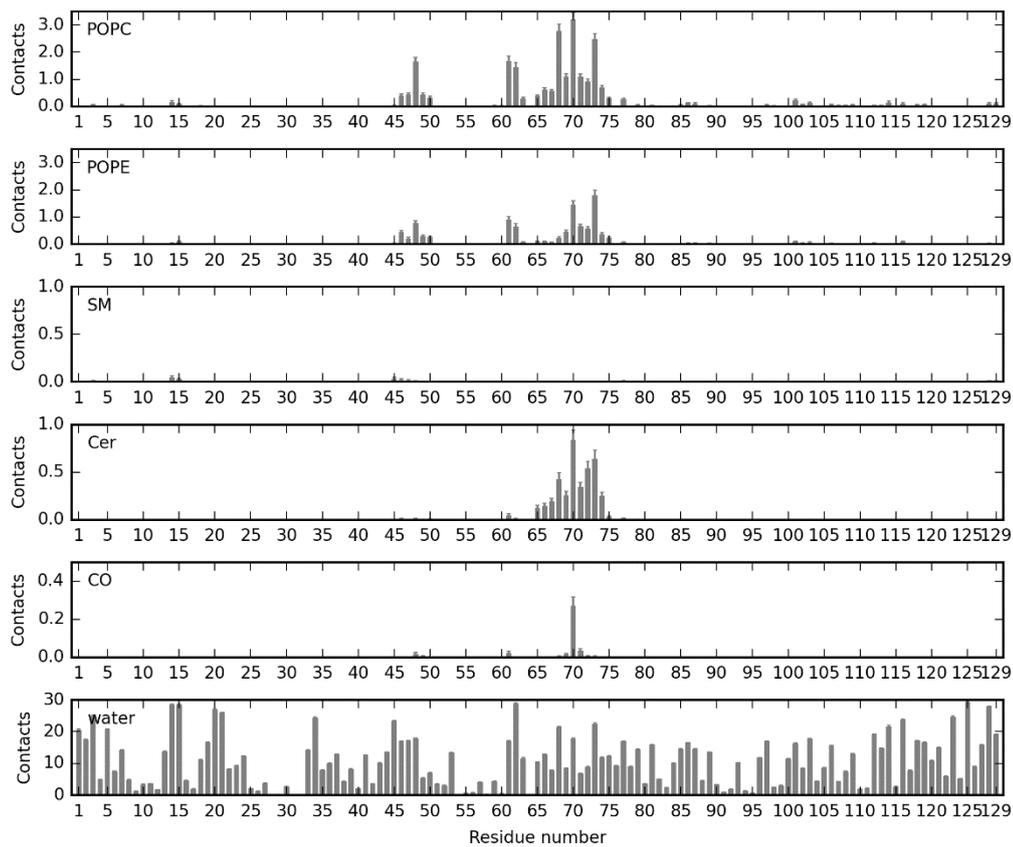
Fig. 5. Contacts of individual lysozyme residues with lipids and water under equilibrium at APPL=0.67 nm^2 employing 0.8 nm cutoff.
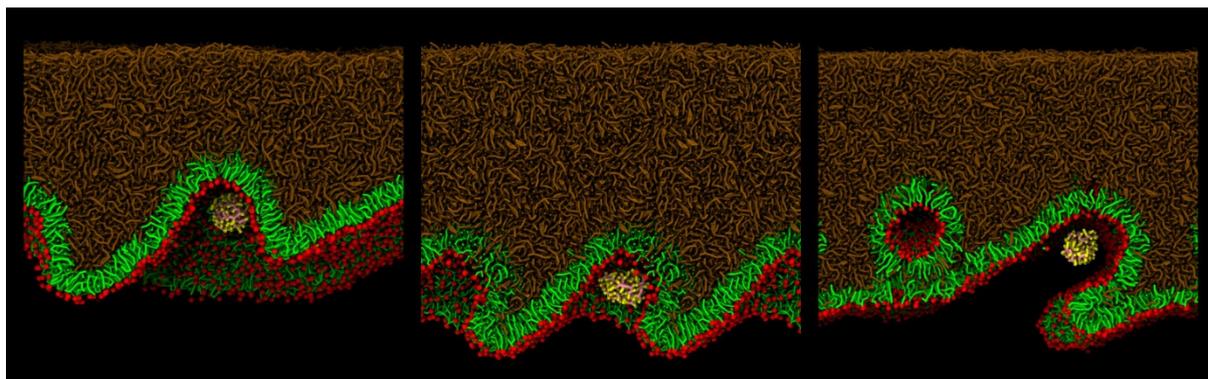
Fig. 6. Representative snapshots taken from three independent non-equilibrium MD trajectories depicting partial embedding of lysozyme into TFLL. The color coding is the same as in Fig. 1, with water molecules not shown for clarity.
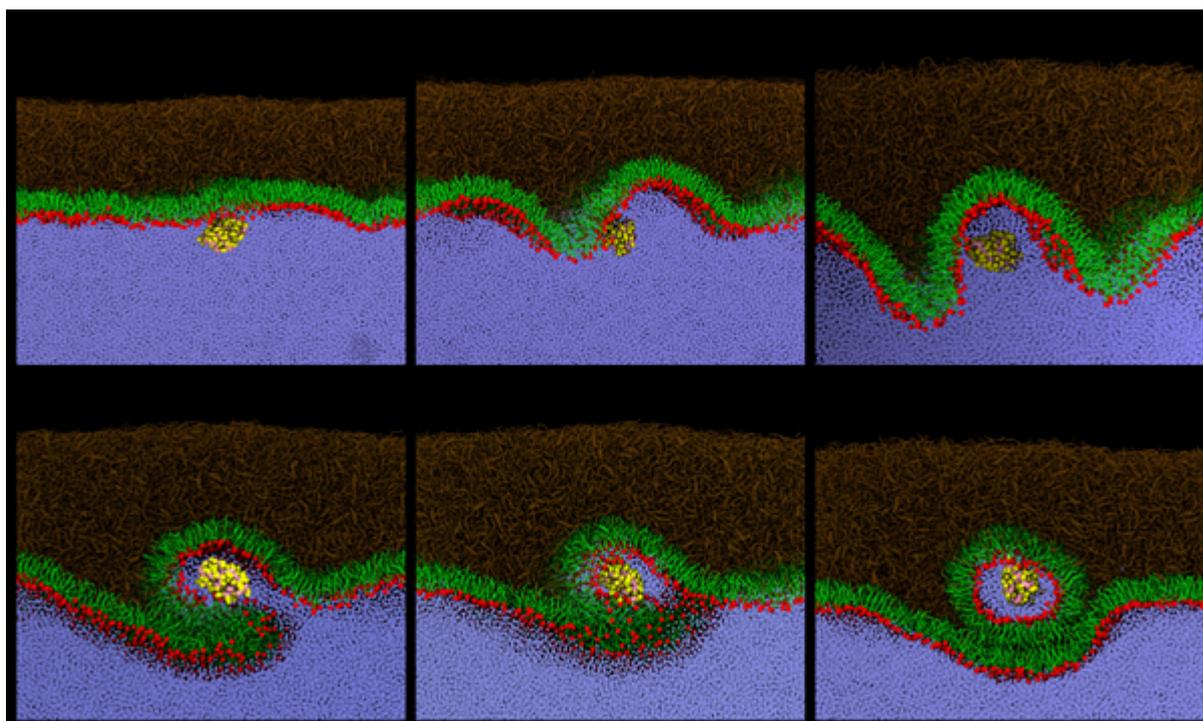
Fig. 7. Representative snapshots taken along one of non-equilibrium MD trajectories where full encapsulation of lysozyme in an inverse micelle occurred. The panels depict consecutively selected snapshots taken during the lateral compression of TFLL and incorporation of the protein within the surface film. The color coding is the same as in Fig. 1.
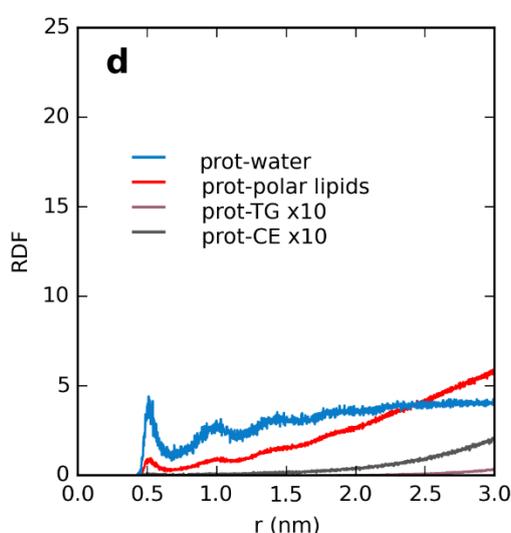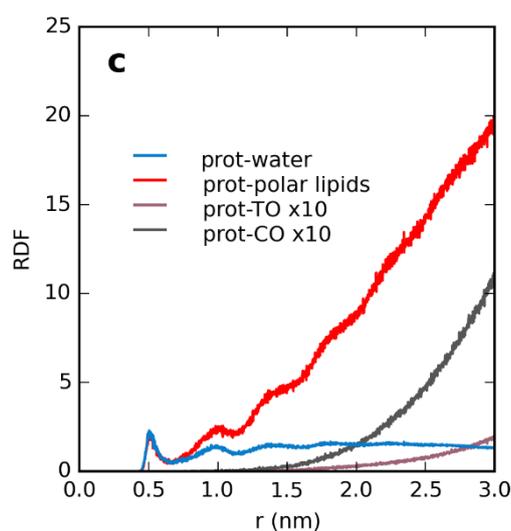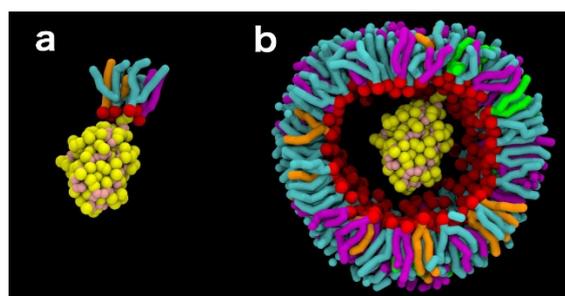
Fig. 8. Two representative snapshots depicting lysozyme molecule together with the nearest polar lipid molecules being a part of the invers micelle in the nonpolar sublayer of TFLL within the distance 0.8 (a) and 2.5 nm (b). Lysozyme is shown in yellow and pink, headgroups of polar lipids in red, tails of POPC in cyan, tails of POPE in magenta, tails of SM in orange, and tails of Cer in green. Water and nonpolar lipids are not shown for clarity. Radial distribution function calculated for the embedded lysozyme and different lipid classes are shown (c) together with the same data for the protein non-embedded (adsorbed at the water-lipid interface) (d). Note that RDFs do not converge to 1 because the system is inhomogeneous. The curves for TG and CO are multiplied ten-fold for enabling direct comparison among all data.
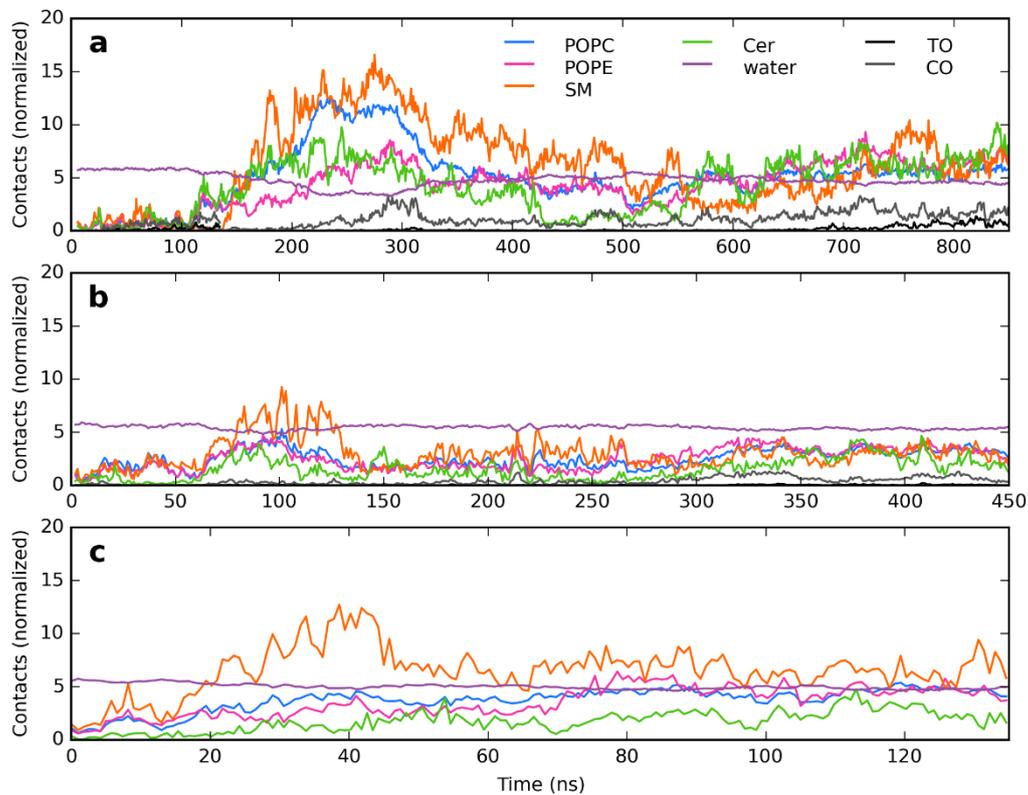
Fig. 9. Contacts between lysozyme and lipids vs time calculated along the three independent non-equilibrium MD trajectories where full embedding of the protein into inverse micelles occurred. The contacts are calculated employing 2.5 nm cutoff and are normalized (divided) per number of given lipids (in the case of polar lipids) and per an arbitrary constant for nonpolar lipids and water (for not normalized data see Fig. S4 in SI).

Graphical Abstract Image
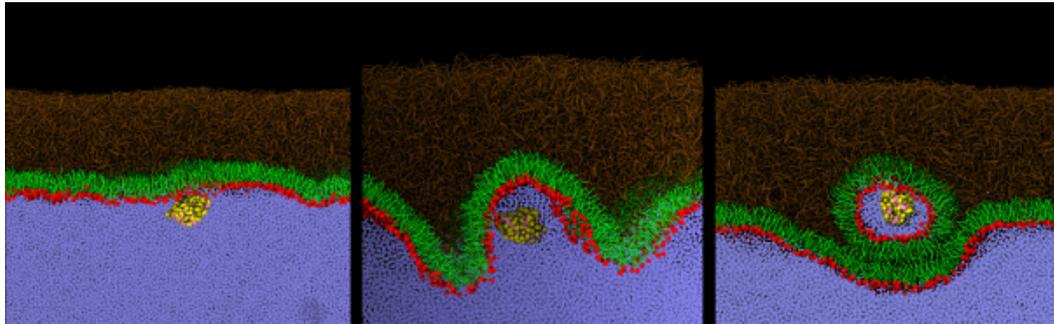
Supplementary Figures
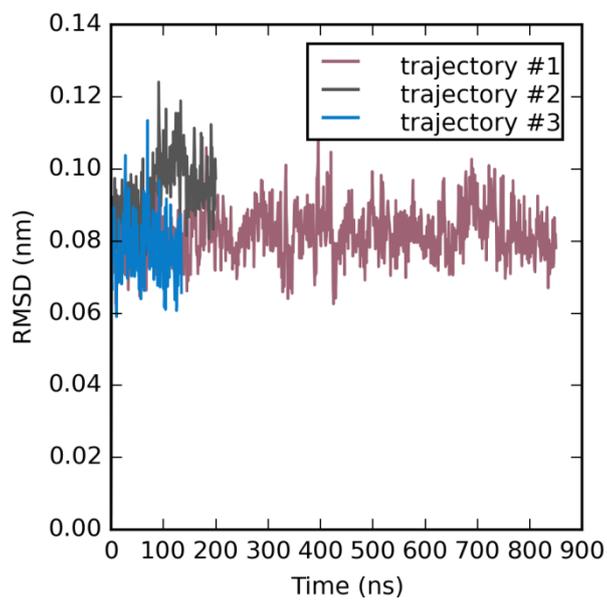
Fig. S1. Root mean square deviation of atom distances in time calculated for lysozyme backbone atoms along the three non-equilibrium MD trajectories with full encapsulation of the protein into TFLL.
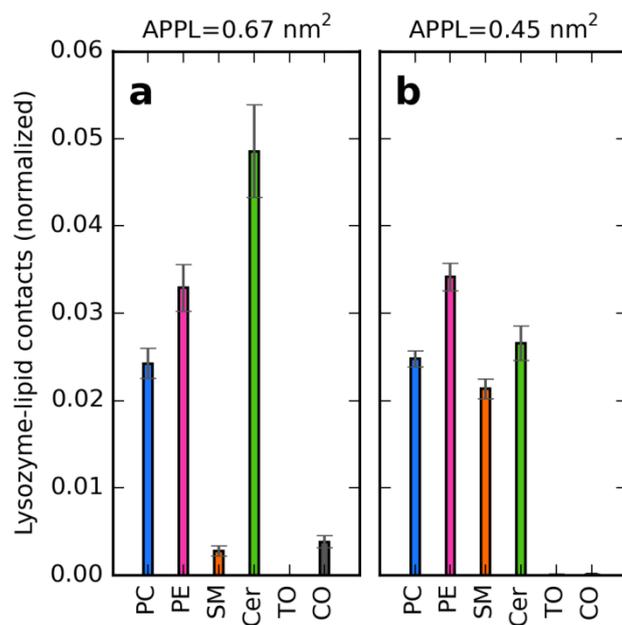
Fig. S2. Lysozyme-lipid contacts under equilibrium in laterally relaxed and compressed TFLL calculated employing 0.8 nm cutoff. To account for binding preferences with interfacial polar lipids, the numbers of contacts are normalized by the number of the given lipids in the system. In the case of non-polar TO and CO, an arbitrary normalization is employed consistently as these lipids do not form a monolayer at the interface.
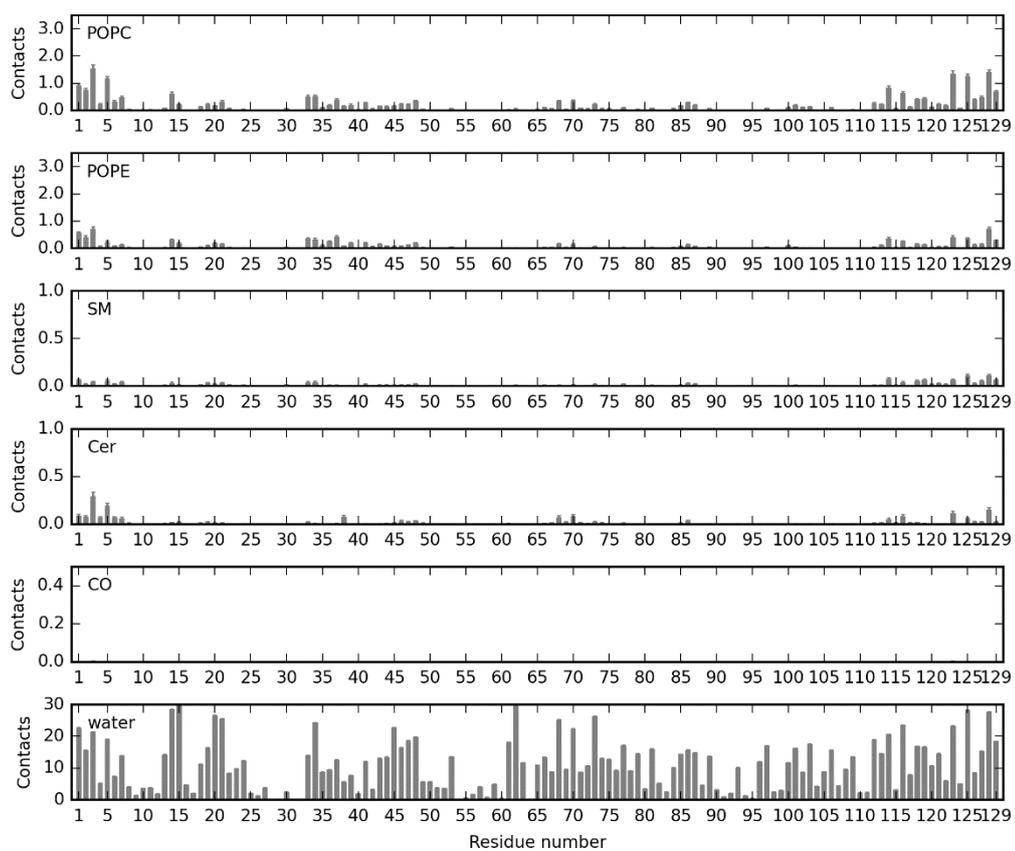
Fig. S3. Contacts of individual lysozyme residues with lipids and water under equilibrium at APPL=0.45 nm^2, employing 0.8 nm cutoff.
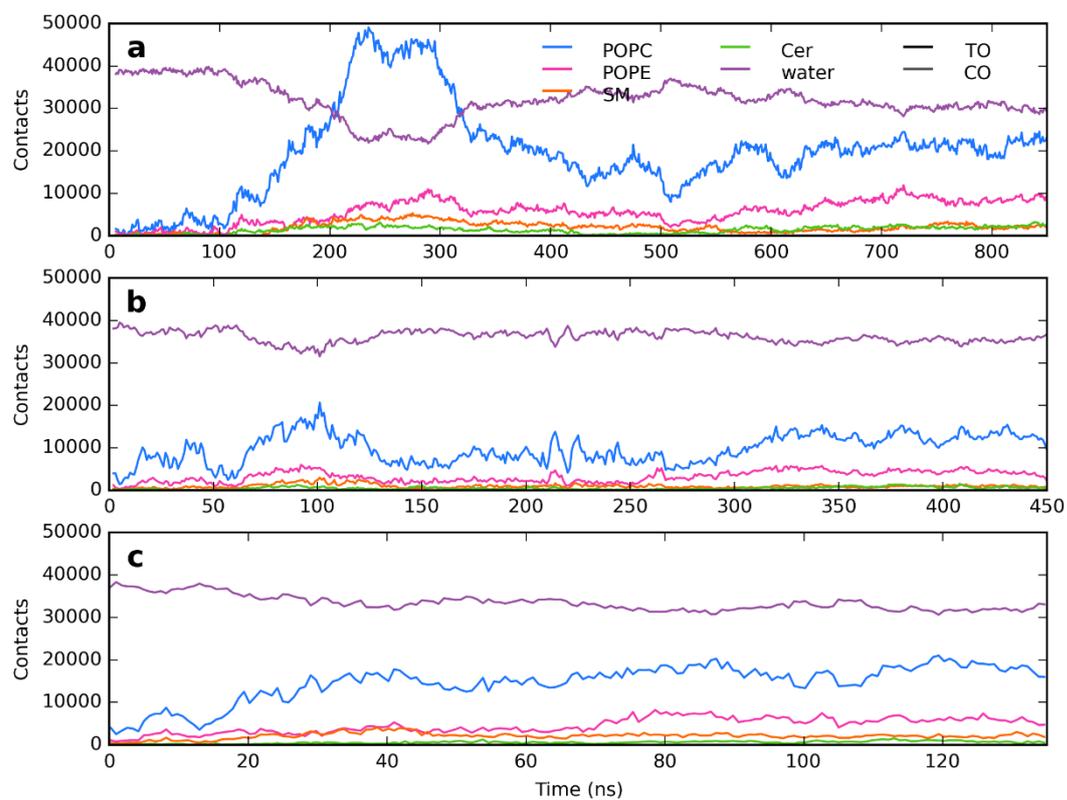
Fig. S4. Contacts between lysozyme and lipids vs time calculated along the three independent non-equilibrium MD trajectories where full embedding of the protein into inverse micelles occurred. The contacts are calculated employing 2.5 nm cutoff.
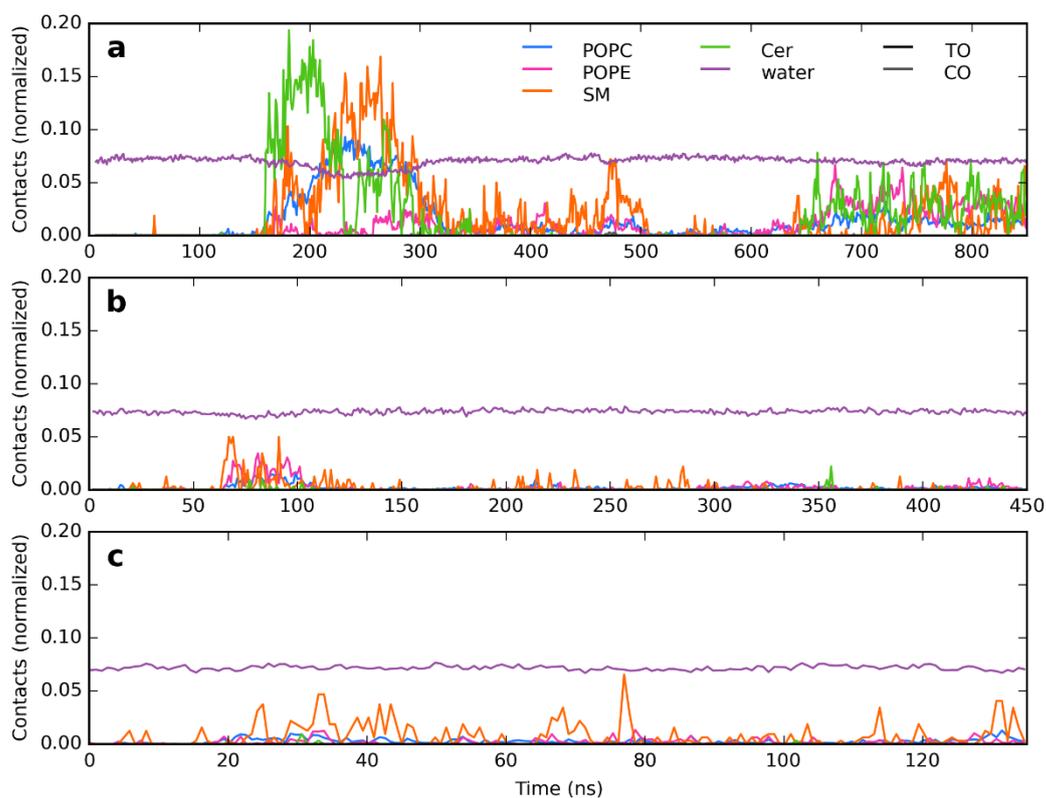
Fig. S5. Contacts between lysozyme and lipids vs time calculated along the three independent non-equilibrium MD trajectories where full embedding of the protein into inverse micelles occurred. The contacts are calculated employing 0.8 nm cutoff and are normalized (divided) per number of given lipids (in the case of polar lipids) and per an arbitrary constant for nonpolar lipids and water.
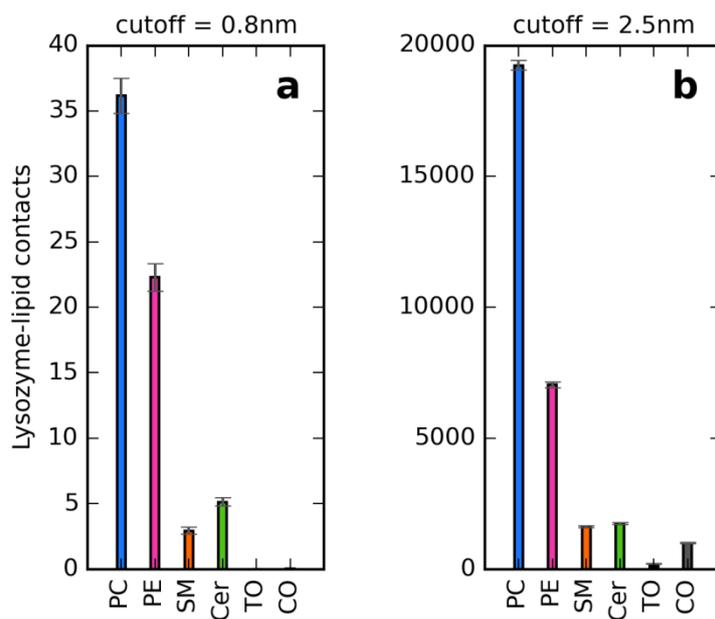
Fig. S6. Lysozyme-lipid contacts under equilibrium upon lysozyme encapsulation in an inverse micelle of polar lipids with the cutoff of 0.8 (a) and 2.5 nm (b). Error bars represent standard error of the data.